JCTC Journal of Chemical Theory and Computation

Article

pubs.acs.org/JCTC

Absorption and Emission Spectra of Solvated Molecules with the EOM−CCSD−PCM Method

Marco Caricato*

Gaussian, Inc., 340 Quinnipiac St. Bldg. 40, Wallingford, Connecticut 06492, United States

ABSTRACT: The accurate calculation of transition energies and properties of isolated molecules is not enough for realistic simulations of their absorption and emission spectra in solution. In fact, the solvent influences the solute geometry, electronic structure, and response to external fields, and a proper description of the solvent effect is fundamental. However, the computational cost of including explicit solvent molecules around the solute becomes rather onerous when an accurate method such as the equation of motion coupled cluster singles and doubles (EOM−CCSD) is employed. The polarizable continuum model of solvation (PCM) may provide an efficient alternative to explicit models, since the sampling of solvent configurations is implicit and the solute−solvent mutual polarization is naturally accounted for. In this contribution, the absorption and emission spectra of molecules in solution are modeled through the EOM−CCSD−PCM method. The equilibrium solvation regime is employed for the geometry optimization of the solute molecule in the ground and excited states, while the nonequilibrium solvation regime is employed for vertical transitions. The theory, implementation, and prototypical applications of the method are presented. The numerical tests involve solvents that are particularly challenging for PCM: low-polar and protic polar solvents. Nonetheless, the experimental trends are well reproduced, and the overall agreement with the measured data is remarkable.

1. INTRODUCTION

The simulation of molecular absorption and emission spectra is fundamental for the characterization of electronic excited states, and accurate methods such as the equation of motion coupled cluster singles and doubles (EOM−CCSD)[1−6] are necessary to obtain reliable simulations.[7,8] However, the spectra of solvated species often show a solvatochromic shift of the bands due to the effect of the solvent on the energy and geometry of the ground as well as the excited states. Obviously, an explicit inclusion of the solvent at the same level of theory of the solute is computationally unfeasible, and some approximation must be introduced.

Many classical models are available to introduce the solvent effect in high-level correlation methods. Some use an atomistic representation of the solvent,[9−19] while others use an implicit representation, such as the polarizable continuum model (PCM).[20−34] Both approaches offer advantages and disadvantages. Explicit models preserve the atomistic picture of the solvent and can describe direct solute−solvent interaction (e.g., strong hydrogen bonds) but require large conformational sampling of the solvent molecules (and thus many expensive CC calculations) to reach convergence on the value of a property. Also, it is difficult to perform geometry optimizations of excited states in solution (to compute adiabatic transition energy or vertical emission energy), especially when the solvent strongly influences the minimum geometry of the solute. On the other hand, continuum models lose the atomistic nature of the solvent and express the conformational average through a macroscopic property of the solvent (e.g., the dielectric permittivity ε in PCM). The advantage is the reduction of the computational cost of the calculation and the natural inclusion of mutual solute−solvent polarization. This also provides a direct way to perform geometry optimizations of solvated molecules in their electronic excited states. The development of such models of solvation for coupled cluster methods is an active and essential research area with the scope of extending the applicability of this level of theory to solvated systems. Most likely, the best of the two worlds is obtained by a combination of explicit (for the first few solvation shells) and implicit models (for the bulk). At present, however, the focus is on the development of the direct coupling of CC methods with either of the solvation approaches.

The coupling of CCSD and PCM was proposed by Cammi[29] with the perturbation theory energy and density approach (PTED),[35,36] which requires the calculation of the CCSD reduced one-particle density matrix (1PDM) to compute the correlation solvent response (i.e., the solvent reaction field). The approximate PTE scheme was also proposed,[29] where the correlation reaction field is neglected (and thus the dependence on the CCSD density) and the solvent effect is only taken into account at the reference wave function level (Hartree−Fock, HF). Later, two intermediate schemes between PTED and PTE were introduced[32] where only part of the CCSD 1PDM (i.e., the single T amplitudes) is used for the correlation reaction field: PTE(S) and PTES (where the S stands for singles). For electronic excited states, I developed the coupling of EOM−CCSD and PCM within the PTED scheme[34] and derived the corresponding approximations for the PTE, PTE(S), and PTES schemes. In ref 34, only the so-called equilibrium solvation regime is considered. In this regime, the solvent is assumed to readjust instantaneously to changes in the solute charge distribution. This is a good assumption for geometry optimizations of excited states, since the relaxation of the solute geometry after an electronic transition happens at the same time scale of the solvent motion. However, this is not a good assumption for vertical electronic transition processes in

Received: August 7, 2012

dx.doi.org/10.1021/ct3006997 | J. Chem. Theory Comput. XXXX, XXX, XXX−XXX

the Franck−Condon regime. In this case, in fact, the time scale of the electronic motion is of the order of 10^{-15} s, thus much faster than orientational motion of the solvent molecules (10^{-12} s). This difference in time scales defines the nonequilibrium solvation regime.

In continuum models, the nonequilibrium solvation is described phenomenologically by dividing the solvent polarization (i.e., the apparent charges $\bar{\mathbf{Q}}$ in PCM) in two components: a "fast" component, which is able to respond to the changes in the solute density (ρ); and a "slow" component, which is kept frozen in equilibrium with the initial solute density. In a vertical electronic (de)excitation process, only the solvent electrons are assumed to be able to respond to the solute density change, while the solvent nuclei are not. The scope of this paper is to develop the nonequilibrium version of the EOM−CCSD−PCM and CCSD−PCM schemes mentioned above to compute vertical absorption and emission spectra. This, together with the equilibrium solvation approach in ref 34 allows for a complete characterization of electronic spectra in solution within the PCM framework.

The paper is organized as follows. The theory and implementation of the methods is presented in Section 2. Numerical applications on test systems and a comparison with experimental data are described in Section 3, while a discussion of the results and concluding remarks are presented in Section 4.

2. THEORY

The nonequilibrium solvation regime can be described in PCM with two equivalent schemes, denoted partition I and II in Table 2 of ref 21. The two schemes differ in the expressions for the fast and slow solvent responses and free energy but provide the same values for the total solvent polarization and free energy.[37] In this work, I use partition II because it involves simpler expressions. In this nonequilibrium scheme, the fast solvent polarization (labeled "dynamic") is computed by replacing ε with the optical dielectric permittivity of the solvent (ε_∞). The slow polarization, labeled "inertial", is computed as the difference between the equilibrium and dynamic polarizations:

$$\bar{\mathbf{Q}}_{\mathrm{in}}(\rho, \varepsilon, \varepsilon_\infty) = \bar{\mathbf{Q}}(\rho, \varepsilon) - \bar{\mathbf{Q}}_{\mathrm{dyn}}(\rho, \varepsilon_\infty) \tag{1}$$

Indicating with i and f the solute initial and final states, respectively, and dropping the explicit dependence of $\bar{\mathbf{Q}}$ on the density and dielectric permittivity, the total nonequilibrium polarization is

$$\bar{\mathbf{Q}}^{\mathrm{neq}} = \bar{\mathbf{Q}}^{\mathrm{f}}_{\mathrm{dyn}} + \bar{\mathbf{Q}}^{\mathrm{i}}_{\mathrm{in}} \tag{2}$$

The free energy expression in this scheme is

$$G^{\mathrm{neq}} = E^{\mathrm{f}} + \frac{1}{2}\bar{\mathbf{V}}^{\mathrm{f}}\cdot\bar{\mathbf{Q}}^{\mathrm{f}}_{\mathrm{dyn}} + \bar{\mathbf{V}}^{\mathrm{f}}\cdot\bar{\mathbf{Q}}^{\mathrm{i}}_{\mathrm{in}} - \frac{1}{2}\bar{\mathbf{V}}^{\mathrm{i}}\cdot\bar{\mathbf{Q}}^{\mathrm{i}}_{\mathrm{in}} \tag{3}$$

where E^{f} is the solute energy in the final state and $\bar{\mathbf{V}}$ is the electrostatic potential on the cavity surface. The free energy in eq 3 is computed with a self-consistent procedure where mutual polarization is achieved between the solute density of the final state and the dynamic solvent response, while the inertial reaction field of the initial state is kept frozen. In other words, the solute density of the final state is "equilibrated" with the dynamic solvent response in the frozen field of the inertial polarization. In an electronic vertical absorption to the state K, i refers to the ground state and f to the state K, while it is the opposite for the electronic vertical emission from the state K.

In the following sections, I present the explicit expressions for the nonequilibrium vertical absorption and emission with the EOM−CCSD−PCM and CCSD−PCM methods according to the complete PTED scheme and the approximate PTE, PTE(S), and PTES schemes. Note that, for the frozen-reaction-field (FRF) scheme, introduced in ref 34, where the PCM response is frozen in equilibrium with the reference wave function, no nonequilibrium scheme can be defined, and the CCSD and EOM−CCSD equations are the same as in the gas phase.

The methods presented in the next two sections are implemented in a development version of the Gaussian suite of programs.[38]

2.1. Absorption. In absorption, the final state f is the Kth excited state, while the initial state i is the ground state. When the solute is treated at the CC level, the PCM charges can be divided in a contribution from the reference wave function (usually Hartree−Fock, HF) and a correlation contribution (from the CC reduced 1PDM). If this division is done before that in "in" and "dyn" charges, and one assumes that no post-HF terms appear in the HF equations (i.e., no PCM charges from the CC reduced density appear in the HF equations), one recognizes that

$$\begin{aligned}\bar{\mathbf{Q}}^{\mathrm{f}}_{0,\mathrm{dyn}} &= \bar{\mathbf{Q}}^{\mathrm{i}}_{0,\mathrm{dyn}}\\ \bar{\mathbf{Q}}^{\mathrm{f}}_{0,\mathrm{in}} &= \bar{\mathbf{Q}}^{\mathrm{i}}_{0,\mathrm{in}}\end{aligned} \tag{4}$$

where the subscript 0 refers to the reference wave function. The nonequilibrium free energy in eq 3 can be rewritten as the following:

$$G^{\mathrm{neq}} = G_{\mathrm{ref}} + \Delta E^{\mathrm{f}} + \frac{1}{2}\bar{\mathbf{V}}^{\mathrm{f}}_{\mathrm{N}}\cdot\bar{\mathbf{Q}}^{\mathrm{f}}_{\mathrm{N,dyn}} + \bar{\mathbf{V}}^{\mathrm{f}}_{\mathrm{N}}\cdot\bar{\mathbf{Q}}^{\mathrm{i}}_{\mathrm{N,in}} - \frac{1}{2}\bar{\mathbf{V}}^{\mathrm{i}}_{\mathrm{N}}\cdot\bar{\mathbf{Q}}^{\mathrm{i}}_{\mathrm{N,in}} \tag{5}$$

where G_{ref} is the equilibrium reference free energy, ΔE^{f} is the correlation and excitation energy, and the subscript N (for normal-product) indicates the dependence only on the correlation density. In this approach, all the nonequilibrium solvent response is taken into account in the CC equations. Also, since in vertical transitions the solute nuclear frame does not move, the solvent response to the solute nuclei distribution can be included in the reference PCM charges. This approach is reasonable for vertical excitations, since the ground state should be the same for the equilibrium and nonequilibrium calculations. Therefore, the nonequilibrium free energy in eq 5 becomes, for the PTED scheme

$$\begin{aligned}G^{\mathrm{PTED,neq}}_K = {} & G_{\mathrm{ref}} + \langle\Phi_0|L_K[\mathrm{e}^{-T}H^{\mathrm{PCM}}_{\mathrm{N}}\mathrm{e}^{T}, R_K]|\Phi_0\rangle\\ & + \langle\Phi_0|(1+\Lambda_K)\mathrm{e}^{-T}H^{\mathrm{PCM}}_{\mathrm{N}}\mathrm{e}^{T}|\Phi_0\rangle\\ & + \omega_K(1 - \langle\Phi_0|L_K R_K|\Phi_0\rangle) + \frac{1}{2}\bar{\mathbf{V}}^{K}_{\mathrm{N}}\cdot\bar{\mathbf{Q}}^{K}_{\mathrm{N,dyn}}\\ & + \bar{\mathbf{V}}^{K}_{\mathrm{N}}\cdot\bar{\mathbf{Q}}^{0}_{\mathrm{N,in}} - \frac{1}{2}\bar{\mathbf{V}}^{0}_{\mathrm{N}}\cdot\bar{\mathbf{Q}}^{0}_{\mathrm{N,in}}\end{aligned} \tag{6}$$

The Kth excited-state potential and charges ($\bar{\mathbf{V}}^{K}_{\mathrm{N}}$ and $\bar{\mathbf{Q}}^{K}_{\mathrm{N,dyn}}$, respectively) depend on the EOM−CCSD reduced 1PDM:

dx.doi.org/10.1021/ct3006997 | J. Chem. Theory Comput. XXXX, XXX, XXX−XXX

$$\bar{\gamma}^{K}_{pq} = \langle\Phi_0|L_K[e^{-T}\{p^{\dagger}q\}e^{T}, R_K]|\Phi_0\rangle + \langle\Phi_0|(1+\Lambda_K)e^{-T}\{p^{\dagger}q\}e^{T}|\Phi_0\rangle \quad (7)$$

where p and q are two generic molecular orbitals. In eqs 6 and 7, Φ_0 is the reference wave function, T is the CC excitation operator, and Λ_K is a deexcitation operator similar to that of gradient theory.[2−4] ω_K is the Kth eigenvalue (and L_K and R_K the corresponding eigenvectors) of the similarity transformed Hamiltonian, $e^{-T}H^{PCM}_N e^{T}$, which contains the PCM operator with the reference charges:

$$H^{PCM}_N = H_N + V_N\cdot\bar{Q}_0 \quad (8)$$

The dynamic charges $\bar{Q}^{K}_{N,dyn}$ are computed in the same way as in ref 34 except for the substitution $\varepsilon \to \varepsilon_\infty$.

Similar to the equilibrium case, the free energy in eq 6 is computed by minimizing the functional with respect to the T, Λ_K, R_K, L_K amplitudes and ω_K. The explicit form of the amplitude equations is the same as that of the equilibrium case in ref 34 when the equilibrium charges $\bar{Q}^{K}_N$ are replaced by the nonequilibrium charges in eq 2. At convergence, the free energy expression in eq 6 reduces to

$$G^{PTED,neq}_K = G_{ref} + \Delta E^{neq}_K + \omega_K - \frac{1}{2}\bar{V}^{K}_N\cdot\bar{Q}^{K}_{N,dyn} - \frac{1}{2}\bar{V}^{0}_N\cdot\bar{Q}^{0}_{N,in} \quad (9)$$

where

$$\Delta E^{neq}_K = \langle\Phi_0|e^{-T}H^{PCM}_N e^{T}|\Phi_0\rangle + \langle\Phi_0|e^{-T}V_N e^{T}|\Phi_0\rangle\cdot(\bar{Q}^{K}_{N,dyn} + \bar{Q}^{0}_{N,in}) \quad (10)$$

As for the equilibrium solvation case, the PTED scheme has the disadvantage that the correlation PCM term couples the T equations with the EOM equations. Thus, the T amplitudes are different for the ground and excited states, and transition energies can only be computed as the difference between energies from the two separate calculations: the nonequilibrium excited state energy and the equilibrium ground state energy. Additionally, the Λ_K equations need to be solved to compute the 1PDM in eq 7, contrary to gas phase EOM−CCSD where Λ_K is only needed for the evaluation of analytic energy gradients.[2−4]

In ref 34, I developed a series of approximate schemes that decouple the T equations from the EOM equations. The same schemes can be extended to the nonequilibrium solvation, thus allowing the computation of transition energies in one step. The approximation derives from neglecting specific terms in the density in eq 7. As shown in ref 34, the reaction field (and similarly the electrostatic potential) can be divided in three contributions:

$$\bar{Q}^{K}_N = \tilde{Q}^{K}_N + \tilde{Q}^{T}_N + \tilde{Q}^{\Lambda}_N \quad (11)$$

where

$$\tilde{Q}^{K}_N = \langle\Phi_0|L_K[e^{-T}Q_N e^{T}, R_K]|\Phi_0\rangle \quad (12)$$

$$\tilde{Q}^{T}_N = \langle\Phi_0|e^{-T}Q_N e^{T}|\Phi_0\rangle \quad (13)$$

$$\tilde{Q}^{\Lambda}_N = \langle\Phi_0|\Lambda_K e^{-T}Q_N e^{T}|\Phi_0\rangle \quad (14)$$

The three approximate schemes, PTE, PTE(S), and PTES, differ in which contribution to the PCM energy term in eq 6 is neglected. The same choices for the equilibrium case can be repeated here.

For PTE, only the $\bar{V}^{K}_N\ \bar{Q}^{K}_{N,dyn}$ term is maintained. Also, no inertial contribution is present, since no correlation reaction field is considered in the ground state with this scheme. Thus, eq 6 becomes

$$G^{PTE,neq}_K = G_{ref} + \langle\Phi_0|L_K[e^{-T}H^{PCM}_N e^{T}, R_K]|\Phi_0\rangle + \langle\Phi_0|(1+\Lambda_K)e^{-T}H^{PCM}_N e^{T}|\Phi_0\rangle + \omega_K(1 - \langle\Phi_0|L_K R_K|\Phi^0\rangle) + \frac{1}{2}\tilde{V}^{K}_N\cdot\tilde{Q}^{K}_{N,dyn} \quad (15)$$

The ground-state equations are the same as the equilibrium case,[29] while for the excited state the only difference is that the PCM charges are computed with ε_∞ instead of ε. At convergence, the nonequilibrium absorption energy, ΔG^{neq} is simply

$$\Delta G^{neq} = \omega_K - \frac{1}{2}\tilde{V}^{K}_N\cdot\tilde{Q}^{K}_{N,dyn} \quad (16)$$

In the PTE(S) scheme, the excited-state dynamic reaction field is approximated as

$$\bar{Q}^{K}_{N,dyn} \simeq \tilde{Q}^{TK}_{N,dyn} = \tilde{Q}^{K}_{N,dyn} + \tilde{Q}^{T}_{N,dyn} \quad (17)$$

while the initial (ground) state inertial reaction field and electrostatic potential are

$$\bar{Q}^{i}_{N,in} \simeq \tilde{Q}^{T}_{N,in} \qquad \bar{V}^{i}_N \simeq \tilde{V}^{T}_N \quad (18)$$

The nonequilibrium solvation free energy in eq 6 becomes

$$G^{PTE(S),neq}_K = G_{ref} + \langle\Phi_0|L_K[e^{-T}H^{PCM}_N e^{T}, R_K]|\Phi_0\rangle + \langle\Phi_0|(1+\Lambda_K)e^{-T}H^{PCM}_N e^{T}|\Phi_0\rangle + \omega_K(1 - \langle\Phi_0|L_K R_K|\Phi_0\rangle) + \frac{1}{2}\tilde{V}^{TK}_N\cdot\tilde{Q}^{TK}_{N,dyn} + \tilde{V}^{TK}_N\cdot\tilde{Q}^{T}_{N,in} - \frac{1}{2}\tilde{V}^{T}_N\cdot\tilde{Q}^{T}_{N,in} \quad (19)$$

By minimizing eq 19 with respect to variations of the Λ_K amplitudes, one finds that the ground state T equations are the same as for the PTE(S) equilibrium case,[32] while the excited-state equilibrium reaction field in the EOM equations is replaced by

$$\tilde{Q}^{TK}_N \to \tilde{Q}^{T}_N + \tilde{Q}^{K}_{N,dyn} \quad (20)$$

Note that the $\bar{Q}^{T}_N$ charges in eq 20 are the ground-state equilibrium charges, and the dynamic part is only needed for the K charges. At convergence, the expression of the transition energy is the same as in eq 16.

For the PTES scheme, the nonequilibrium free energy of the Kth state is

dx.doi.org/10.1021/ct3006997 | J. Chem. Theory Comput. XXXX, XXX, XXX−XXX

$$G_K^{\mathrm{PTES,neq}} = G_{\mathrm{ref}} + \langle\Phi_0|L_K[\mathrm{e}^{-T}H_{\mathrm{N}}^{\mathrm{PCM}}\mathrm{e}^{T}, R_K]|\Phi_0\rangle + \langle\Phi_0|(1+\Lambda_K)\mathrm{e}^{-T}H_{\mathrm{N}}^{\mathrm{PCM}}\mathrm{e}^{T}|\Phi_0\rangle + \omega_K(1-\langle\Phi_0|L_KR_K|\Phi_0\rangle) + \frac{1}{2}\tilde{\mathbf{V}}_{\mathrm{N}}^{TK}\cdot\tilde{\mathbf{Q}}_{\mathrm{N,dyn}}^{TK} + \tilde{\mathbf{V}}_{\mathrm{N}}^{\Lambda}\cdot\tilde{\mathbf{Q}}_{\mathrm{N,dyn}}^{T} + \bar{\mathbf{V}}_{\mathrm{N}}^{K}\cdot\tilde{\mathbf{Q}}_{\mathrm{N,in}}^{T} - \frac{1}{2}\tilde{\mathbf{V}}_{\mathrm{N}}^{T}\cdot\tilde{\mathbf{Q}}_{\mathrm{N,in}}^{T} \quad (21)$$

The ground-state PTES T equations are still the same as the corresponding equilibrium case,[32] while the EOM equations use the same substitution as in eq 20 for the nonequilibrium reaction field. At convergence, the transition energy is that in eq 16 also for this scheme.

For the three approximate schemes, the ground-state equations are not affected by the nonequilibrium solvation. The decoupling of the T and L_K/R_K equations thus allows the calculation of transition energies in one step, contrary to the PTED scheme. Additionally, it is not necessary to solve the Λ_K equations, since these also are decoupled from the T, L_K, and R_K equations. From an implementation perspective, minimal changes to the equilibrium code is required, and the same terms presented in ref 34 appear here (with the proper nonequilibrium PCM charges).

2.2. Emission. In emission, the initial state i is the Kth excited state while the final state f is the ground state. Contrary to the absorption case, it is not a good assumption to separate the reference from the correlation reaction field before introducing the separation between dynamic and inertial polarization. In fact, the ground-state reference wave function is strongly influenced by the field of inertial charges deriving from the equilibrium excited-state calculation (in other words, the approximation in eq 4 is not valid). For the ground state in the PTED scheme, the nonequilibrium free energy expression in eq 3 becomes

$$G_0^{\mathrm{PTED,neq}} = \langle\Phi_0|(1+\Lambda)\mathrm{e}^{-T}H\mathrm{e}^{T}|\Phi_0\rangle + \frac{1}{2}\bar{\mathbf{V}}^{0}\cdot\bar{\mathbf{Q}}_{\mathrm{dyn}}^{0} + \bar{\mathbf{V}}^{0}\cdot\bar{\mathbf{Q}}_{\mathrm{in}}^{K} - \frac{1}{2}\bar{\mathbf{V}}^{K}\cdot\bar{\mathbf{Q}}_{\mathrm{in}}^{K} \quad (22)$$

where

$$\bar{\mathbf{V}}^{0} = \langle\Phi_0|(1+\Lambda)\mathrm{e}^{-T}\mathbf{V}\mathrm{e}^{T}|\Phi_0\rangle$$
$$\bar{\mathbf{Q}}_{\mathrm{dyn}}^{0} = \langle\Phi_0|(1+\Lambda)\mathrm{e}^{-T}\mathbf{Q}_{\mathrm{dyn}}\mathrm{e}^{T}|\Phi_0\rangle \quad (23)$$

By introducing now the separation between reference and normal-product operators for the ground-state quantities and rearranging the terms, eq 22 can be recast as

$$G_0^{\mathrm{PTED,neq}} = G_{\mathrm{ref}}^{\mathrm{neq}} + \frac{1}{2}\bar{\mathbf{V}}_{\mathrm{N}}^{0}\cdot\bar{\mathbf{Q}}_{\mathrm{N,dyn}}^{0} + \langle\Phi_0|(1+\Lambda)\mathrm{e}^{-T}H_{\mathrm{N}}^{\mathrm{PCM,neq}}\mathrm{e}^{T}|\Phi_0\rangle \quad (24)$$

where $G_{\mathrm{ref}}^{\mathrm{neq}}$ is the nonequilibrium reference free energy:

$$G_{\mathrm{ref}}^{\mathrm{neq}} = \langle\Phi_0|H|\Phi_0\rangle + \frac{1}{2}\bar{\mathbf{V}}_0\cdot\bar{\mathbf{Q}}_{0,\mathrm{dyn}} + \bar{\mathbf{V}}_0\cdot\bar{\mathbf{Q}}_{\mathrm{in}}^{K} - \frac{1}{2}\bar{\mathbf{V}}^{K}\cdot\bar{\mathbf{Q}}_{\mathrm{in}}^{K} \quad (25)$$

and the reference dynamic charges and electrostatic potential are

$$\bar{\mathbf{Q}}_{0,\mathrm{dyn}} = \langle\Phi_0|\mathbf{Q}_{\mathrm{dyn}}|\Phi_0\rangle$$
$$\bar{\mathbf{V}}_0 = \langle\Phi_0|\mathbf{V}|\Phi_0\rangle \quad (26)$$

The nonequilibrium PCM Hamiltonian operator in normal-product form contains the contribution from the reference dynamic charges and the Kth state inertial charges:

$$H_{\mathrm{N}}^{\mathrm{PCM,neq}} = H_{\mathrm{N}} + \mathbf{V}_{\mathrm{N}}\cdot(\bar{\mathbf{Q}}_{0,\mathrm{dyn}} + \bar{\mathbf{Q}}_{\mathrm{in}}^{K}) \quad (27)$$

$G_{\mathrm{ref}}^{\mathrm{neq}}$ in eq 25 can be computed by solving the nonequilibrium HF equations,[39−41] where the inertial charges are kept constant during the iterative procedure. Once these equations are solved, the PCM contribution to the normal-product Hamiltonian in eq 27 is contained into the diagonal Fock operator (i.e., the orbital energies) and does not add any new term to the CC equations for the ground-state equilibrium case.

The expression for the nonequilibrium free energy in eq 24 is very similar to that for the equilibrium case.[29,31] The only difference is that the correlation charges $\bar{\mathbf{Q}}_{\mathrm{N,dyn}}^{0}$ are computed using ε_∞ instead of ε . Therefore, the same equations for the T and Λ amplitudes occur.[29,31] Another consequence is that all the approximate schemes derived from PTED (i.e., PTE, PTE(S), and PTES)[32] maintain the same equilibrium expressions when $\varepsilon \to \varepsilon_\infty$. Therefore, the same equilibrium code for the ground state can be used for the vertical emission calculations provided that the reference wave function is computed within the nonequilibrium regime and ε_∞ is used in the correlation reaction field evaluation. Another important difference between the schemes is the definition of inertial charges and Kth state electrostatic potential. This is reported in Table 1. Since, in the FRF scheme, there is no CC reaction field contribution in the excited-state calculation, only the frozen reference reaction field is maintained. Thus, eq 24 reduces to the usual EOM−CCSD expression for the gas phase with the reference wave function computed in the field of the equilibrium PCM charges. In other words, no nonequilibrium scheme can be formulated for FRF.

Table 1. Definitions of the Kth Excited-State Inertial Charges and Electrostatic Potential in the PTED, PTES, PTE(S), PTE, and FRF Schemes for Nonequilibrium Vertical Emission

	$\bar{\mathbf{Q}}_{\mathrm{in}}^{\mathrm{i}}$	$\bar{\mathbf{V}}^{\mathrm{i}}$
PTED	$(\bar{\mathbf{Q}}_0 + \bar{\mathbf{Q}}_{\mathrm{N}}^{K})$	$\bar{\mathbf{V}}_0 + \bar{\mathbf{V}}_{\mathrm{N}}^{K}$
PTES	$(\bar{\mathbf{Q}}_0 + \bar{\mathbf{Q}}_{\mathrm{N}}^{TK})_{\mathrm{in}}$	$\bar{\mathbf{V}}_0 + \bar{\mathbf{V}}_{\mathrm{N}}^{TK}$
PTE(S)	$(\bar{\mathbf{Q}}_0 + \bar{\mathbf{Q}}_{\mathrm{N}}^{TK})_{\mathrm{in}}$	$\bar{\mathbf{V}}_0 + \bar{\mathbf{V}}_{\mathrm{N}}^{TK}$
PTE	$(\bar{\mathbf{Q}}_0 + \bar{\mathbf{Q}}_{\mathrm{N}}^{K})_{\mathrm{in}}$	$\bar{\mathbf{V}}_0 + \bar{\mathbf{V}}_{\mathrm{N}}^{K}$
FRF	$\bar{\mathbf{Q}}_{0,\mathrm{in}}$	$\bar{\mathbf{V}}_0$

The evaluation of vertical emission energy requires two separate calculations for the equilibrium excited-state energy and nonequilibrium ground-state energy. However, the computational cost of the latter is negligible compared to that of the geometry optimization of the excited state.

3. NUMERICAL APPLICATIONS

This section reports the calculated vertical electronic absorption and emission energies for two widely studied molecules: *trans*-acrolein and methylenecyclopropene (MCP),[26−28,34,42−51] shown in Figure 1. The optimized structures of the ground and first excited states were obtained with all the CC−PCM schemes in ref 34 and are used here for

dx.doi.org/10.1021/ct3006997 | J. Chem. Theory Comput. XXXX, XXX, XXX−XXX

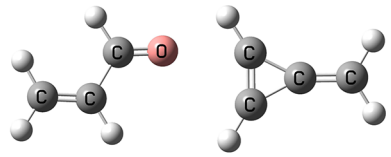

(a) Trans-acrolein (b) MCP

Figure 1. Ground-state structures of *trans*-acrolein and MCP.

the vertical transition calculations. In particular, the lowest two excited states in absorption and the first excited state in emission are considered. For emission, the optimized geometry of the excited state remains planar for acrolein while it is distorted to a C_2 symmetry for MCP, as shown in Figure 2.

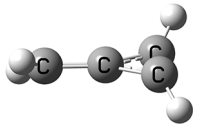

Figure 2. Minimum structure of MCP in the first excited state (C_2 symmetry).

Both molecules are studied with bare PCM in a polar and in a low-polar solvent for which experimental data is available. The polar solvents are water (ε = 78.4; ε_∞ = 1.8) for acrolein and methanol (ε = 32.6; ε_∞ = 1.8) for MCP, while the low-polar solvents are cyclohexane (ε and ε_∞ = 2.0) for acrolein and *n*-pentane (ε and ε_∞ = 1.8) for MCP. All four solvents are challenging for bare PCM solvation, since the polar solvents are protic and may form hydrogen bonds, while the low-polar solvents may induce nonelectrostatic effects for which there is not a proper model for excited states. Nevertheless, a comparison with experimental data can provide useful insights on the ability of such a simple solvation approach to describe solvatochromic shifts. A refined treatment where some explicit solvent molecules from the first solvation shell are included (and possibly treated at a lower level of theory) is a viable strategy but is beyond the scope of this work and is material for following research.

The symmetrical version of the integral equation formalism PCM (IEF−PCM)[52−54] with the continuous surface charge approach of Scalmani and Frisch[55] is used. Two radii definitions are compared to investigate the cavity effect on the transition energy: universal force field (UFF) radii[56] scaled by a factor of 1.1, and solvation model D (SMD) radii.[57] The former are the default in Gaussian[38] because of their availability for most of the periodic table, whereas the scaling factor of 1.1 provides a cavity with a surface close to the solvent excluded surface.[55] The latter were optimized to reproduce experimental solvation free energies.[57] None of them were optimized for excited states; thus, it is interesting to test their performance. The aug-cc-pVDZ basis set[58] is used throughout, and all calculations are performed with a development version of the Gaussian suite of programs.[38]

3.1. *trans*-Acrolein. The vertical absorption energy and solvent shift of acrolein are reported in Table 2 for the first excited state and in Table 3 for the second excited state. For this molecule, experimental data is available for gas phase and solution; thus, it is possible to assess the error introduced by the solvation model.

Table 2. Vertical Absorption Energy and Solvent Shift (eV) for the First Excited State ($n \rightarrow \pi^*$, A″) of Acrolein in Gas, Water, and Cyclohexane

		cyclohexane		water		solvent shift	
A″	gas	UFF	SMD	UFF	SMD	UFF	SMD
exp	3.71[a]	3.71[b]		3.94[c]		+0.23	
PTED	3.88	3.88	3.87	3.97	4.05	+0.09	+0.18
PTES		3.85	3.84	3.95	4.03	+0.10	+0.19
PTE(S)		3.84	3.84	3.94	4.02	+0.10	+0.18
PTE		3.86	3.85	3.98	4.07	+0.12	+0.22
FRF		3.94	3.93	4.04	4.18	+0.10	+0.25

[a]Ref 43. [b]Ref 44. [c]Ref 46.

Table 3. Vertical Absorption Energy and Solvent Shift (eV) for the Second Excited State ($\pi \rightarrow \pi^*$, A′) of Acrolein in Gas, Water, and Cyclohexane

		cyclohexane		water		solvent shift	
A′	gas	UFF	SMD	UFF	SMD	UFF	SMD
exp	6.41[a]	6.11[b]		5.90[c]		−0.21	
PTED	6.80	6.73	6.71	6.64	6.54	−0.09	−0.17
PTES		6.71	6.69	6.61	6.49	−0.10	−0.20
PTE(S)		6.71	6.69	6.61	6.48	−0.10	−0.21
PTE		6.70	6.68	6.59	6.45	−0.11	−0.23
FRF		6.76	6.76	6.65	6.56	−0.09	−0.20

[a]Ref 43. [b]Ref 44. [c]Ref 45.

The gas phase absorption energy for the first transition is well reproduced, with an error of 0.17 eV shown in Table 2. Similar errors are found for cyclohexane, and the difference between the UFF and SMD results is small. The approximate methods are close to the PTED results (within 0.02−0.06 eV), with the largest difference found for FRF. The data for water are also rather good, with the UFF results very close to experiment. However, this is a fortuitous cancellation of errors, since the error is smaller than in the gas phase. On the other hand, SMD provides an error of 0.11 eV with the PTED scheme and a solvation energy shift of 0.18 eV, in very good agreement with the experimental one of 0.23 eV (compared to the 0.09 eV with UFF radii). The approximate methods behave fairly well. Among these, FRF is the furthest from PTED (0.13 eV for water with SMD). Note that the UFF results compare well with those computed with SAC−CI/PCM and a similar cavity by Fukuda et al.,[28] who reported a solvent shift of 0.11 eV.

The agreement with the experiment in the gas phase is not as good for the second transition, with a difference of 0.39 eV as shown in Table 3. This can be attributed to vibronic effects, since this transition is of $\pi \rightarrow \pi^*$ character and eventually leads to a rotation of the terminal CH_2 group out of the molecular plane, with a mixing of the ground and the excited states. These vibronic effects are neglected in the calculated transition energy and make the experimental value uncertain, thus contributing to the difference between the two. However, here, we are more interested in the solvatochromic shift and in the additional error introduced by the solvation model. The calculated data in cyclohexane provide the right trend compared to the experiment when passing from gas phase to solution by reducing the magnitude of the transition energy. The error is of the order of 0.6 eV compared to the experiment; thus, it increases the discrepancy already found for the gas phase and discussed above. The difference between the PCM schemes and

dx.doi.org/10.1021/ct3006997 | J. Chem. Theory Comput. XXXX, XXX, XXX−XXX

cavity definition is much smaller than all these other factors. For water, the trend is again reproduced compared to the gas phase and cyclohexane. The errors with UFF is larger (~0.70 eV) than with SMD, which is comparable to that in cyclohexane. This is reasonable, since the UFF radii are longer than those of SMD; thus, the effect of water (which is considerable for this transition) is smaller. As a consequence, the experimental water−cyclohexane shift (−0.21 eV) in Table 3 is very well reproduced by all the PCM schemes with the SMD cavity, while it is half in magnitude with UFF (and consistent with the SAC−CI result: −0.09 eV[28]).

The vertical emission energy for the first excited state is reported in Table 4. The geometry, which is planar for this state, is optimized with the corresponding PCM scheme. On the other hand, the second excited state is not considered because of the mixing with the first excited state when the CH_2 group rotates out of plane, as discussed above. For this transition, only experimental data for a low-polar solvent is available (2-methyl-THF at 77 K[47]). Therefore, no comparison is possible for solvent shifts. Nonetheless, Table 4 reports the emission energy computed with all the methods in both solvents, since this is useful for an internal comparison of the various approximations. For the low-polar solvent, the agreement of all methods with the available experimental data is rather good. The PTED result is in the middle of the experimental large band, for which three small picks can be distinguished. The difference between SMD and UFF is small for this solvent. Larger differences start to appear between PTED and the approximate schemes compared to the vertical absorption energy: −0.09 eV for PTES, −0.10 eV for PTE(S), −0.05 eV for PTE, and +0.11 eV for FRF. This difference increases for water: −0.35 eV for PTES, −0.40 eV for PTE(S), −0.13 eV for PTE, and +0.73 eV for FRF with SMD. The difference between UFF and SMD also increases due to the smaller cavity (thus larger solvent effect) of SMD. The solvent shift is also very different between PTED and the other methods. The closest approximate method to PTED is PTE for both cavity definitions. PTE(S) and PTES provide shifts that are more than twice in magnitude that of PTED but with the right sign. On the other hand, FRF provides large shifts with the opposite sign.

In order to distinguish the effect on the geometry from that on the energy, emission energies are recomputed for all the schemes at the PTED optimized geometry and reported in Table 5. The data in the table show that the gap from the PTED results is shortened for all methods but the trend does not change. In fact, PTE(S) and PTES still provide values of the solvent shift that are more than twice that of PTED, and FRF still provides the opposite sign of the shift. Thus, the effect of the PCM approximations on the energy seems larger than that on the geometry.

Table 4. Vertical Emission Energy and Solvent Shift (eV) for the First Excited State ($n \rightarrow \pi^*$, A″) of Acrolein in Gas, Water, and Cyclohexane[a]

		cyclohexane		water		solvent shift	
A″	gas	UFF	SMD	UFF	SMD	UFF	SMD
exp		(3.31, 3.26, 3.00)[b]					
PTED	3.15	3.17	3.17	3.08	3.02	−0.09	−0.15
PTES		3.08	3.08	2.81	2.67	−0.27	−0.41
PTE(S)		3.06	3.07	2.77	2.62	−0.29	−0.45
PTE		3.12	3.12	2.96	2.89	−0.16	−0.23
FRF		3.29	3.28	3.54	3.75	+0.25	+0.47

[a]The geometry is optimized with the corresponding PCM scheme. [b]Ref 47.

Table 5. Vertical Emission Energy and Solvent Shift (eV) for the First Excited State ($n \rightarrow \pi^*$, A″) of Acrolein in Water and Cyclohexane[a]

	cyclohexane		water		solvent shift	
A″	UFF	SMD	UFF	SMD	UFF	SMD
PTED	3.17	3.17	3.08	3.02	−0.09	−0.15
PTES	3.11	3.11	2.90	2.76	−0.21	−0.35
PTE(S)	3.10	3.10	2.88	2.74	−0.22	−0.36
PTE	3.13	3.13	2.99	2.91	−0.14	−0.22
FRF	3.26	3.24	3.44	3.67	+0.18	+0.43

[a]The geometry is optimized with the PTED scheme.

3.2. Methylencyclopropene (MCP). The vertical absorption energy and solvent shift of MCP are reported in Table 6 for the first excited state and in Table 7 for the second excited state. In this case, no experimental data in the gas phase is available; thus, it is not possible to assess the intrinsic agreement with EOM−CCSD. Nevertheless, the comparison is possible for the data in solution.

Table 6. Vertical Absorption Energy and Solvent Shift (eV) for the First Excited State ($\pi \rightarrow \pi^*$, B_2) of MCP in Gas, Methanol, and *n*-Pentane

		n-pentane		methanol		solvent shift	
B_2	gas	UFF	SMD	UFF	SMD	UFF	SMD
exp		4.01[a]		4.49[a]		+0.48	
PTED	4.48	4.44	4.43	4.58	4.64	+0.14	+0.21
PTES		4.36	4.32	4.52	4.57	+0.16	+0.25
PTE(S)		4.35	4.31	4.52	4.56	+0.17	+0.25
PTE		4.37	4.33	4.56	4.62	+0.19	+0.29
FRF		4.58	4.62	4.75	4.89	+0.17	+0.27

[a]Ref 48.

Table 7. Vertical Absorption Energy and Solvent Shift (eV) for the Second Excited State ($\pi \rightarrow \pi^*$, A_1) of MCP in Gas, Methanol, and *n*-Pentane

		n-pentane		methanol		solvent shift	
A_1	gas	UFF	SMD	UFF	SMD	UFF	SMD
exp		6.02[a]		5.90[a]		−0.12	
PTED	6.15	6.13	6.10	6.10	6.10	−0.03	0.00
PTES		6.12	6.09	6.10	6.10	−0.02	+0.01
PTE(S)		6.11	6.08	6.10	6.09	−0.01	+0.01
PTE		6.12	6.09	6.10	6.10	−0.02	+0.01
FRF		6.15	6.15	6.12	6.14	−0.03	−0.02

[a]Ref 48.

The agreement for the low-polar solvent is rather poor for the first transition energy, shown in Table 6. The difference varies from ~0.40 eV for PTED to ~0.30 eV for the approximate schemes to ~0.60 eV for FRF. In this case, the difference may be due to nonelectrostatic contributions neglected in the excited-state calculations as well as to

dx.doi.org/10.1021/ct3006997 | J. Chem. Theory Comput. XXXX, XXX, XXX−XXX

uncertainties in the experimental value of the vertical transition energy. The approximate schemes agree with PTED within 0.1 eV, except for FRF (0.14−0.19 eV). The choice of the cavity for this solvent is irrelevant. For the polar solvent, the agreement with experiment improves considerably. The difference in fact is within 0.15 eV except with FRF, for which it is 0.27 eV with UFF and 0.40 with SMD. The agreement is in general better with UFF for methanol. However, also in this case, this may be fortuitous considering that the difference between the polar and low-polar solvent is small (due to the large cavity). This is consistent with the values of solvent shift, for which SMD performs better than UFF. The direction of the experimental shift is well reproduced by PCM, but the magnitude is about half of the measured value. This is mainly due to the difference between the experimental and calculated data for the low-polar solvent.

The second transition shows a much smaller solvent shift, as reported in Table 7. This means that this excited state is not much influenced by the presence of the solvent. The computed absolute values for the absorption energy are in reasonable agreement with the experimental data for both solvents and all methods. The sign of the shift is only reproduced with UFF. However, the performance of the continuum model is good in the sense that it correctly predicts that the solvent effect is small for this transition, independently on its polarity. Also, the experimental solvent shift (−0.12 eV in Table 7) is below the expected error of EOM−CCSD. The difference between methods is small, within 0.01−0.05 eV.

The vertical emission energy from the lowest excited state is reported in Table 8. There is no experimental data available;

Table 8. Vertical Emission Energy and Solvent Shift (eV) for the First Excited State ($\pi \rightarrow \pi^*$, B) of MCP in Gas, Methanol, and *n*-Pentane[a]

		n-pentane		methanol		solvent shift	
B	gas	UFF	SMD	UFF	SMD	UFF	SMD
PTED	1.41	1.42	1.43	1.18	1.09	−0.24	−0.34
PTES		1.23	1.20	–	–	–	–
PTE(S)		1.19	1.15	–	–	–	–
PTE		1.33	1.31	1.01	0.90	−0.32	−0.41
FRF		1.63	1.69	1.95	2.14	+0.32	+0.45

[a]The geometry is optimized with the corresponding PCM scheme.

therefore, the comparison is only internal to the methods. The minimum has a C_2 symmetry, shown in Figure 2. This is still the first excited state in most cases, except for PTE(S) and PTES in methanol where this state becomes the ground state and it is not possible to compute the emission energy. For *n*-pentane, the difference between PTED and the approximate schemes is 0.20−0.30 eV, and the best agreement is obtained with PTE. For methanol, PTE is still in good agreement with PTED, whereas FRF is off by 0.77 eV with UFF and 1.05 eV with SMD. The PTED solvent shift is also well reproduced by PTE, while the sign is opposite with FRF.

When the vertical emission calculation is repeated at the PTED optimized geometry, PTE(S) and PTES provide closer results to PTED in *n*-pentane as it is shown by a comparison between Table 8 and Table 9. Also the FRF−PTED difference becomes smaller. However, the best agreement is still obtained with PTE. The same trend is observed in methanol and consequently in the solvent shift. For the latter, FRF still yields the opposite sign compared to the other methods.

Table 9. Vertical Emission Energy and Solvent Shift (eV) for the First Excited State ($\pi \rightarrow \pi^*$, B) of MCP in Methanol and *n*-Pentane[a]

	n-pentane		methanol		solvent shift	
B	UFF	SMD	UFF	SMD	UFF	SMD
PTED	1.42	1.43	1.18	1.09	−0.24	−0.34
PTES	1.33	1.30	0.90	0.76	−0.43	−0.54
PTE(S)	1.32	1.28	0.88	0.74	−0.44	−0.54
PTE	1.35	1.32	1.00	0.89	−0.35	−0.43
FRF	1.57	1.64	1.85	2.07	+0.28	+0.43

[a]The geometry is optimized with the PTED scheme.

4. DISCUSSION AND CONCLUSIONS

In this work, I report the extension to the nonequilibrium solvation regime of EOM−CCSD−PCM[26,34] and CCSD−PCM[29,31,32] for vertical absorption and emission spectra of solvated molecules. The nonequilibrium energy expressions are derived and implemented for the complete PTED scheme and the approximate PTE, PTE(S), and PTES schemes. All of the above are tested on two representative molecules, acrolein and MCP, for which experimental data is available. Also, the FRF scheme (where the reaction field is frozen at the reference level) is tested.

For acrolein (see Section 3.1), the experimental solvent shifts for vertical absorption energies are well reproduced by PCM (shown in Tables 2 and 3). Also, the calculated values of vertical emission energies are in good agreement with the available experimental data. All of the approximate schemes perform relatively well for absorption energies. The best agreement with PTED is obtained with PTES, and the worst with FRF. The SMD cavity is necessary for reproducing the experimental trends. For emission (Tables 4 and 5), the differences between schemes are more accentuated. PTE provides the best agreement with PTED. PTE(S) and PTES provide the right trends but too large magnitudes. On the contrary, FRF is not even able to reproduce the trends.

Similar considerations apply to the MCP results, reported in Section 3.2. The solvent energy shift for the absorption energy of the lowest excited state is reproduced within a factor of 2 with the SMD cavity (shown in Table 6). The difference is mainly due to the low-polar solvent results. Indeed, the absolute value of the transition energy in methanol is within the expected error of EOM−CCSD (∼0.15 eV). The UFF cavity is too large also in this case, and the values of the solvent shift are about two-thirds of that with SMD. The difference between PTED and the approximate schemes is small (≤0.12 eV) except with FRF (∼0.20 eV). For the transition energy to the second state, PCM predicts a small solvent effect in agreement with the experiment. For emission (Tables 8 and9), PTE(S) and PTES predict a shift between the ground and the first excited state in methanol, contrary to the other schemes. PTE provides the best agreement with PTED in both solvents. On the other hand, FRF predicts the opposite solvent shift compared to all other schemes.

In summary, the difference between the various schemes is relatively small for absorption energies, while it may be significant for emission energies (both in terms of excited state optimized geometry and actual transition energy). For the latter, PTE provides the best agreement with PTED. PTE(S) and PTES predict the correct trends, but the magnitude of the shift is larger than PTED. Also, in one case (MCP in

dx.doi.org/10.1021/ct3006997 | J. Chem. Theory Comput. XXXX, XXX, XXX−XXX

methanol), PTE(S) and PTES fail to reproduce the correct order of the states. FRF has proved largely unreliable by predicting the opposite sign of the solvent shift in emission compared to all other methods for both molecules. Thus, PTE(S) and PTES seem to perform better as ground-state approximations of PTED,[32] while FRF should be avoided altogether. The cavity built with SMD radii provides results in better agreement with experiment than that with UFF (×1.1 scaling factor) radii. The latter cavity is larger, and the solvent effect for polar solvents seems too small.

Overall, the combination of EOM−CCSD and PCM seems to provide rather good agreement with experimental data for absolute energies and solvent energy shifts. The largest difference is found for low-polar solvents, which are difficult to treat with an electrostatic continuum model if non-electrostatic effects are important. In general, however, all the solvents used in this work are challenging for continuum models (the polar solvents, water and methanol, can form hydrogen bonds). Nonetheless, the performance of PCM is remarkable, allowing to account for the solvent effects on both geometry and energy. A better description of specific solute−solvent interaction may be obtained by including some explicit solvent molecules (possibly treated at a lower level of theory than coupled cluster) around the solute and surrounding the whole system with PCM. Efforts in this direction are under way.

AUTHOR INFORMATION

Corresponding Author

*E-mail: marco@gaussian.com.

Notes

The authors declare no competing financial interest.

ACKNOWLEDGMENTS

I wish to thank Dr. Giovanni Scalmani (Gaussian, Inc.) and Prof. Benedetta Mennucci (University of Pisa) for useful discussions.

REFERENCES

(1) Stanton, J. F.; Bartlett, R. J. *J. Chem. Phys.* **1993**, *98*, 7029−7039.
(2) Stanton, J. F. *J. Chem. Phys.* **1993**, *99*, 8840−8847.
(3) Stanton, J. F.; Gauss, J. *J. Chem. Phys.* **1994**, *100*, 4695−4698.
(4) Kallay, M.; Gauss, J. *J. Chem. Phys.* **2004**, *121*, 9257−9269.
(5) Bartlett, R. J.; Musial, M. *Rev. Mod. Phys.* **2007**, *79*, 291−352.
(6) Shavitt, I.; Bartlett, R. J. *Many-Body Methods in Chemistry and Physics*; Cambridge University Press: Cambridge, U.K., 2009.
(7) Caricato, M.; Trucks, G. W.; Frisch, M. J.; Wiberg, K. B. *J. Chem. Theory Comput.* **2010**, *6*, 370−383.
(8) Caricato, M.; Trucks, G. W.; Frisch, M. J.; Wiberg, K. B. *J. Chem. Theory Comput.* **2011**, *7*, 456−466.
(9) Osted, A.; Kongsted, J.; Mikkelsen, K. V.; Christiansen, O. *J. Phys. Chem. A* **2004**, *108*, 8646−8658.
(10) Kongsted, J.; Osted, A.; Pedersen, T. B.; Mikkelsen, K. V.; Christiansen, O. *J. Phys. Chem. A* **2004**, *108*, 8624−8632.
(11) Aidas, K.; Kongsted, J.; Osted, A.; Mikkelsen, K. V.; Christiansen, O. *J. Phys. Chem. A* **2005**, *109*, 8001−8010.
(12) Kowalski, K.; Valiev, M. *J. Phys. Chem. A* **2006**, *110*, 13106−13111.
(13) Fan, P.-D.; Valiev, M.; Kowalski, K. *Chem. Phys. Lett.* **2008**, *458*, 205−209.
(14) Day, P. N.; Jensen, J. H.; Gordon, M. S.; Webb, S. P.; Stevens, W. J.; Krauss, M.; Garmer, D.; Basch, H.; Cohen, D. *J. Chem. Phys.* **1996**, *105*, 1968−1986.
(15) Gordon, M. S.; Freitag, M. A.; Bandyopadhyay, P.; Jensen, J. H.; Kairys, V.; Stevens, W. J. *J. Phys. Chem. A* **2001**, *105*, 293−307.
(16) Bandyopadhyay, P.; Gordon, M. S.; Mennucci, B.; Tomasi, J. *J. Chem. Phys.* **2002**, *116*, 5023−5032.
(17) Sneskov, K.; Schwabe, T.; Kongsted, J.; Christiansen, O. *J. Chem. Phys.* **2011**, *134*, 104108.
(18) Slipchenko, L. V. *J. Phys. Chem. A* **2010**, *114*, 8824−8830.
(19) Kosenkov, D.; Slipchenko, L. V. *J. Phys. Chem. A* **2011**, *115*, 392−401.
(20) Miertus, S.; Scrocco, E.; Tomasi, J. *Chem. Phys.* **1981**, *55*, 117−129.
(21) Tomasi, J.; Mennucci, B.; Cammi, R. *Chem. Rev.* **2005**, *105*, 2999−3093.
(22) Christiansen, O.; Mikkelsen, K. V. *J. Chem. Phys.* **1999**, *110*, 1365−1375.
(23) Christiansen, O.; Mikkelsen, K. V. *J. Chem. Phys.* **1999**, *110*, 8348−8360.
(24) Osted, A.; Kongsted, J.; Mikkelsen, K. V.; Christiansen, O. *Mol. Phys.* **2003**, *101*, 2055−2071.
(25) Kongsted, J.; Pedersen, T. B.; Osted, A.; Hansen, A. E.; Mikkelsen, K. V.; Christiansen, O. *J. Phys. Chem. A* **2004**, *108*, 3632−3641.
(26) Caricato, M.; Mennucci, B.; Scalmani, G.; Trucks, G. W.; Frisch, M. J. *J. Chem. Phys.* **2010**, *132*, 084102.
(27) Cammi, R.; Fukuda, R.; Ehara, M.; Nakatsuji, H. *J. Chem. Phys.* **2010**, *133*, 024104.
(28) Fukuda, R.; Ehara, M.; Nakatsuji, H.; Cammi, R. *J. Chem. Phys.* **2011**, *134*, 104109.
(29) Cammi, R. *J. Chem. Phys.* **2009**, *131*, 164104.
(30) Cammi, R. *Int. J. Quantum Chem.* **2010**, *110*, 3040−3052.
(31) Caricato, M.; Scalmani, G.; Trucks, G. W.; Frisch, M. J. *J. Phys. Chem. Lett.* **2010**, *1*, 2369−2373.
(32) Caricato, M. *J. Chem. Phys.* **2011**, *135*, 074113.
(33) Caricato, M.; Scalmani, G.; Frisch, M. J. *J. Chem. Phys.* **2011**, *134*, 244113.
(34) Caricato, M. *J. Chem. Theory Comput.* **2012**, DOI: 10.1021/ct300382a.
(35) Olivares del Valle, F.; Tomasi, J. *Chem. Phys.* **1991**, *150*, 139−150.
(36) Aguilar, M. A.; Olivares del Valle, F. J.; Tomasi, J. *Chem. Phys.* **1991**, *150*, 151−161.
(37) Aguilar, M. A. *J. Phys. Chem. A* **2001**, *105*, 10393−10396.
(38) Frisch, M. J.; Trucks, G. W.; Schlegel, H. B.; Scuseria, G. E.; Robb, M. A.; Cheeseman, J. R.; Scalmani, G.; Barone, V.; Mennucci, B.; Petersson, G. A.; Nakatsuji, H.; Caricato, M.; Li, X.; Hratchian, H. P.; Izmaylov, A. F.; Bloino, J.; Zheng, G.; Sonnenberg, J. L.; Hada, M.; Ehara, M.; Toyota, K.; Fukuda, R.; Hasegawa, J.; Ishida, M.; Nakajima, T.; Honda, Y.; Kitao, O.; Nakai, H.; Vreven, T.; Montgomery Jr., J. A.; Peralta, J. E.; Ogliaro, F.; Bearpark, M.; Heyd, J. J.; Brothers, E.; Kudin, K. N.; Staroverov, V. N.; Keith, T.; Kobayashi, R.; Normand, J.; Raghavachari, K.; Rendell, A.; Burant, J. C.; Iyengar, S. S.; Tomasi, J.; Cossi, M.; Rega, N.; Millam, J. M.; Klene, M.; Knox, J. E.; Cross, J. B.; Bakken, V.; Adamo, C.; Jaramillo, J.; Gomperts, R.; Stratmann, R. E.; Yazyev, O.; Austin, A. J.; Cammi, R.; Pomelli, C.; Ochterski, J. W.; Martin, R. L.; Morokuma, K.; Zakrzewski, V. G.; Voth, G. A.; Salvador, P.; Dannenberg, J. J.; Dapprich, S.; Parandekar, P. V.; Mayhall, N. J.; Daniels, A. D.; Farkas, O.; Foresman, J. B.; Ortiz, J. V.; Cioslowski, J.; Fox, D. J. *Gaussian Development Version*, Revision H.09+ ed.; Gaussian, Inc.: Wallingford, CT, 2010.
(39) Caricato, M.; Ingrosso, F.; Mennucci, B.; Tomasi, J. *J. Chem. Phys.* **2005**, *122*, 154501.
(40) Caricato, M.; Mennucci, B.; Tomasi, J.; Ingrosso, F.; Cammi, R.; Corni, S.; Scalmani, G. *J. Chem. Phys.* **2006**, *124*, 124520.
(41) Mennucci, B. *Theor. Chem. Acc.* **2006**, *116*, 31−42.
(42) Buswell, A. M.; Dunlop, E. C.; Rodebush, W. H.; Swartz, J. B. *J. Am. Chem. Soc.* **1940**, *62*, 325−328.
(43) Walsh, A. D. *Trans. Faraday Soc.* **1945**, *41*, 498−505.
(44) Mackinney, G.; Temmer, O. *J. Am. Chem. Soc.* **1948**, *70*, 3586−3590.
(45) Forbes, W. F.; Shilton, R. *J. Am. Chem. Soc.* **1959**, *81*, 786−790.
(46) Inuzuka, K. *Bull. Chem. Soc. Jpn.* **1961**, *34*, 729−732.

(47) Becker, R. S.; Inuzuka, K.; King, J. *J. Chem. Phys.* **1970**, *52*, 5164−5170.
(48) Staley, S. W.; Norden, T. D. *J. Am. Chem. Soc.* **1984**, *106*, 3699−3700.
(49) Aquilante, F.; Barone, V.; Roos, B. O. *J. Chem. Phys.* **2003**, *119*, 12323−12334.
(50) Losa, A. M.; Galvan, I. F.; Aguilar, M. A.; Martin, M. E. *J. Phys. Chem. B* **2007**, *111*, 9864−9870.
(51) Aidas, K.; Møgelhøj, A.; Nilsson, E. J. K.; Johnson, M. S.; Mikkelsen, K. V.; Christiansen, O.; Söderhjelm, P.; Kongsted, J. *J. Phys. Chem. A* **2008**, *109*, 8001−8010.
(52) Cances, E.; Mennucci, B.; Tomasi, J. *J. Chem. Phys.* **1997**, *107*, 3032−3041.
(53) Mennucci, B.; Cances, E.; Tomasi, J. *J. Phys. Chem. B* **1997**, *101*, 10506−10517.
(54) Lipparini, F.; Scalmani, G.; Mennucci, B.; Cancès, E.; Caricato, M.; Frisch, M. J. *J. Chem. Phys.* **2010**, *133*, 014106.
(55) Scalmani, G.; Frisch, M. J. *J. Chem. Phys.* **2010**, *132*, 114110.
(56) Rappe, A. K.; Casewit, C. J.; Colwell, K. S.; Goddard, W. A.; Skiff, W. M. *J. Am. Chem. Soc.* **1992**, *114*, 10024−10035.
(57) Marenich, A. V.; Cramer, C. J.; Truhlar, D. G. *J. Phys. Chem. B* **2009**, *113*, 6378−6396.
(58) Dunning, T. H. *J. Chem. Phys.* **1989**, *90*, 1007−1023.